Nonlinear beam steering by fractional vortex dipoles

Georgi Maleshkov,[1] Dragomir N. Neshev,[2] and Alexander Dreischuh[1,2]

[1]*Department of Quantum Electronics, Sofia University, Sofia 1164, Bulgaria*

[2]*Nonlinear Physics Centre, Research School of Physical Sciences and Engineering, Australian National University,*

Canberra, Australian Capital Territory 0200, Australia

We study the ability of beams with complex phase dislocations to guide and steer signal beams in self-focusing nonlinear media. In particular, we report on the experimental demonstration of signal deflection by beams carrying step-screw phase dislocation in the form of a fractional vortex dipole. We show how the beam deflection can be ruled by the geometry and orientation of the dipole.

I. INTRODUCTION

Propagation of optical beams in nonlinear media (NLM) has been a subject of continuing interest for more than 4 decades due to the possibility for creation of reconfigurable waveguides through the intensity-dependent refractive index change [1,2]. Such optically induced waveguides can guide weak signal beams and pulses [3,4], which motivates the investigation of novel techniques for manipulation of the transverse beam dynamics and correspondingly opens possibilities for realization of waveguides with complex geometries.

Optical beams can be spatially manipulated by introducing chirp to their transverse phase profiles [5–7]. Therefore, the implementation of steering schemes utilizing beams with complex spatial phase profile, in the form of phase singularities [8], appears especially attractive. An example of such a beam is an optical vortex with its helical phase profile described by $\exp(im\vartheta)$ multiplier, where ϑ is the azimuthal coordinate and m is the vortex topological charge. Due to the presence of a point phase singularity in the beam center, the optical vortices are associated with intrinsic energy flow and orbital angular momentum [9]. Propagation of optical vortices in nonlinear media has received great attention with their ability to form bright or dark optical vortex solitons (OVSs) in self-focusing and self-defocusing nonlinear media, respectively [2,10,11].

In a self-defocusing medium, OVSs can guide signal beams in their core [12–14]. Therefore by controlling the position of an optical vortex core, one can effectively steer a signal beam. The transverse velocity of an OVS has a radial and an angular component arising from the transverse phase and intensity gradients, respectively [15,16]. Two practical ways to control the vortex position have their origin in the Guoy phase shift on both sides of a background beam waist [16,17] and in the interaction of ordered structures of OVSs [18] controlled by their topological charges.

Though the OVS is a stationary and stable nonlinear state in self-defocusing media, other schemes implementing nonstationary (moving) two-dimensional dark solitons have also shown great abilities for manipulation of signal beams. The possibility to branch a single input probe beam into ordered structures of sub-beams by quasi-two-dimensional dark spatial solitons has been demonstrated numerically in [19].

Other branching and steering schemes have also been realized by employing the inherent dynamics of ring dark solitary waves [20–22] or the decay of higher-order vortices [23]. Finally, dark beams containing mixed step-screw phase dislocation [i.e., π semispirals separated by a one-dimensional (1D) phase step] have shown important potential for signal beam steering due to their defined spatial velocity, controlled through geometrical parameters [24–26].

Despite the large activities on beam steering in defocusing nonlinear materials, manipulation of signals by beams with complex phase structure in *self-focusing nonlinear media* remains unexplored. This is somewhat surprising since self-focusing materials are more common in nature. However, the implementation of beams with phase singularities for beam steering in self-focusing media has been hindered by the intrinsic azimuthal and modulational instabilities. Due to such instabilities, the OVS experiences breakup into a number of fundamental solitons that fly away from the vortex center [28–31].

In this work, we show that such instabilities are not a limiting factor for beam steering when beams with mixed phase dislocations are utilized. We demonstrate experimentally and describe theoretically the ability of such beams, also called *fractional vortex dipoles*, to steer signals in a self-focusing nonlinear medium. In particular, we employ the self-focusing photorefractive nonlinearity in a biased strontium barium niobate (SBN) crystal and demonstrate bright signal beam deflection that can be controlled by the geometrical parameters of the fractional vortex dipole.

II. BASIC CONCEPT

A fractional vortex dipole or mixed step-screw phase dislocation consists of a one-dimensional phase step of a finite length, which ends, by necessity, with a pair of phase semispirals with opposite helicities [24,25] [Fig. 1 (left)]. In contrast to an optical vortex, the phase gradient of the spiral phase caps can be noninteger, or fractional, that reflects to the notation of a fractional vortex dipole. Here, we consider a fractional vortex dipole with a step-screw (SS) phase dislocation [26]. The phase profile of such a dipole is depicted in Fig. 1 (left) and described by
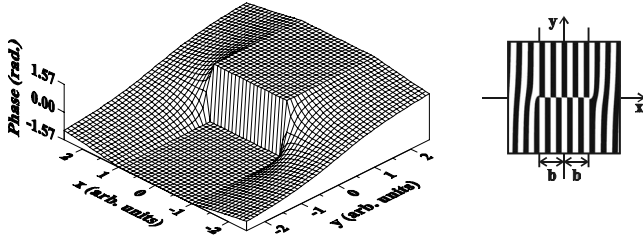
FIG. 1. Phase profile of the step-screw mixed phase dislocation (left) and structure of the corresponding computer-generated hologram (right).

$$\Phi(x,y) = \Delta\Phi\left[\frac{(1-\alpha)\mathrm{sgn}(y)}{2} - \frac{\beta}{\pi}\tan^{-1}\left(\frac{\alpha y}{x+b\beta}\right)\right], \quad (1)$$

where $\alpha=0$ for $|x| \leq b$; $\alpha=1$ and $\beta=-1$ or 1 for $x>b$ and $x<-b$, respectively. $\Delta\Phi$ stands for the magnitude of the phase jump at the origin, $2b$ is the dipole length, and x and y are the transverse coordinates. While the particular phase structure of SS fractional vortex dipole has a discontinuity of the derivative of the phase at positions $x= \pm b$, other types of phase profile without such discontinuity can also be defined [26]. However, the particular phase definition does not change qualitatively their propagation dynamics. Experimentally, the only controllable way to produce such fractional vortex dipole is by a computer-generated hologram (CGH) [Fig. 1 (right)].

Beams containing fractional vortex dipoles are inherently restless. Their linear propagation exhibits a transverse velocity $V_\perp$, depending on both the length $2b$ and the magnitude of the phase jump $\Delta\Phi$. The transverse motion of the beam is due to the phase gradients perpendicular to the one-dimensional phase step. While, at the initial evolution stage (0–0.1 Rayleigh diffraction lengths), the phase semispirals are strongly reshaping [26], at longer propagations, $V_\perp$ remains nearly constant [26,27].

In self-focusing nonlinear media, a bright trailing peak is formed next to phase dislocation in the course of propagation. However, its transverse motion is bounded to the dynamics of the phase dislocation. Due to the nonlinear index change, this peak will induce an optical waveguide which direction and curvature can be controlled by the orientation of the phase singularity. In a photorefractive crystal, one can expect that if written at a photosensitive wavelength, such a waveguide will be able to guide and steer more powerful signal beams at nonphotosensitive wavelengths [32].

III. EXPERIMENTAL RESULTS AND NUMERICAL SIMULATIONS

To demonstrate this concept, in our experiments we use a continuous-wave frequency-doubled $\mathrm{Nd:YVO_4}$ laser at a wavelength of 532 nm. The schematic of the experimental setup is shown in Fig. 2. A fractional vortex dipole of 110 μm length and $\Delta\Phi=\pi$ is generated by a binary CGH [see Fig. 1 (right)] fabricated photolithographically with a grating period of 30 μm. The first-order diffracted beam carrying the phase dislocation is imaged and demagnified by an
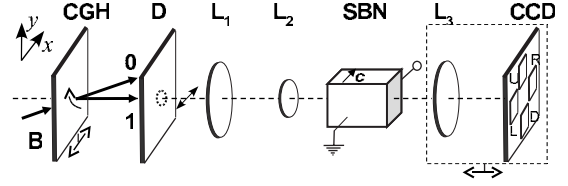

FIG. 2. Experimental setup. B: Gaussian background beam illuminating the CGH. D: diaphragm selecting the first-order diffracted beam with the fractional vortex dipole. L_1 and L_2: lenses forming an inverted telescope; SBN: biased photorefractive crystal with marked orientation of the c axis. Horizontal arrow: beam's polarization. L_3 and CCD: imaging lens and charge-coupled device camera moving on a common translation stage to image the input or output facet of the crystal. The four virtual output channels are sketched in the plane of the CCD array.

inverse telescope $L_1–L_2$ to 35 μm at the front face of a 20 mm long SBN photorefractive crystal (Fig. 2). The polarization of the laser beam is parallel to the crystalline c axis, thus the beam experiences a strong photorefractive nonlinearity due to the high electro-optic coefficient r_{33} in the SBN. The crystal is biased by an externally applied electric field ($E_0 \sim 1000$ V/m). The front or the back face of the crystal is imaged with a lens L_3 onto a charge-coupled device (CCD) camera, both moving on a common translation stage (see Fig. 2). Special attention is paid to the alignment of the CGH in order to maintain unchanged position of the central part of the encoded SS dislocation with respect to the illuminating beam. The hologram was also rotated stepwise by 90° around its center. Thanks to the relatively long (tens of seconds) response time of the self-focusing photorefractive nonlinearity, we could use the same laser beam as a signal beam. For this purpose, the CGH is quickly shifted horizontally (represented by the arrow at the bottom of the CGH in Fig. 2) in order to illuminate the homogeneous side portion of the binary structure, consisting of parallel stripes only. Without any other change in the alignment, the distribution of the guided signal beam is recorded on the CCD camera no later than 2 s after writing of the induced waveguide. Additionally, we have also assured that even at twice longer sensing period, the Gaussian signal beam is not able to noticeably affect the induced waveguide.

To numerically simulate the beam propagation inside the biased photorefractive SBN crystal (dc field applied along the x direction, being parallel to the crystalline c axis), we modeled the following equations [33,34]:

$$i\frac{\partial A_j}{\partial z} + \frac{1}{2}\left(\frac{\partial^2}{\partial x^2} + \frac{\partial^2}{\partial y^2}\right)A_j - \gamma(E_{sc} + E_0)A_j = 0, \quad (2)$$

where A_j is the jth component of the slowly varying optical-field amplitude and $\gamma=\frac{1}{2}(2\pi/\lambda)^2 x_0^2 n_0^4 r_{\mathrm{eff}}$ is a material nonlinear parameter accounting for the corresponding term of the electro-optic tensor ($r_{\mathrm{eff}}=r_{33}$ for SBN). $\gamma>0$ accounts for the self-focusing nonlinear response of the crystal. E_{sc} is the space-charge field related to the electrostatic potential $\phi(E_{sc}=-\partial\phi/\partial x)$. E_0 is the external field applied along the c axis perpendicular to the propagation direction. All transverse coordinates are expressed in units of the beam width
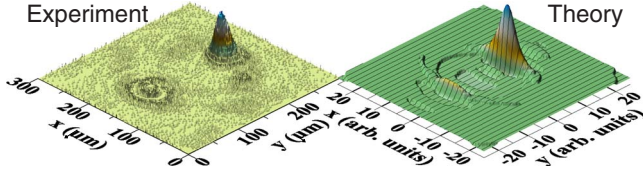
FIG. 3. (Color online) Experimental (left) and numerically simulated (right) pump beam profiles ($|A_1|^2$) at the exit of the SBN crystal for deflection to the upper channel U in Fig. 2. $\Delta\Phi = \pi$ and $2b = 35$ μm.

x_0, whereas the propagation coordinate z is expressed in units of the Rayleigh diffraction length $L_{\text{Diff}} = (2\pi/\lambda)n_0 x_0^2$. The electrostatic potential ϕ is modeled by the equation [33,34]

$$\nabla^2\phi + \nabla\phi\nabla\ \ln(1 + I) = E_0\frac{\partial}{\partial x}\ln(1 + I), \quad (3)$$

where $I = |A_1|^2 + |A_2|^2$ is the total light intensity normalized to the dark irradiance of the SBN crystal. The last term in Eq. (3) accounts for the drift of the charge carriers. In the above notations, the refractive index of the medium is modulated via the Pockels effect according to the relation $n^2 = n_0^2 + n_0^4 r_{33}\partial\phi/\partial x$, assuming that the incident beams are polarized along x direction (c crystalline axis). All material parameters taken in the numerical simulations correspond to the typical values of SBN crystals [35,36] ($r_{33} = 180$ pm/V and $n_0 = 2.3$). For our experimental conditions, $x_0 = 17$ μm and $\gamma = 4.3.10^{-4}$ m/V.

The slowly varying electric-field amplitude of the beam carrying the fractional vortex dipole is assumed to be tanh-shaped and of the form

$$A_1(x, y, z = 0) = B(x, y)\tanh[r_{\alpha,\beta}(x, y)]\exp[i\Phi(x, y)], \quad (4)$$

where the effective radial coordinate $r_{\alpha,\beta}$ is given by

$$r_{\alpha,\beta} = [\alpha(x + \beta b)^2 + y^2]^{1/2} \quad (5)$$

and the super-Gaussian background beam is

$$B(x, y) = B_0\exp\{-[\sqrt{(x^2 + y^2)/w^2}]^{14}\}, \quad (6)$$

where w is chosen to be more than 10 times larger than the deflection of the bright self-focusing peak at the exit of the nonlinear crystal. The input signal beam is assumed to be Gaussian-shaped and equal in width to the background carrying the fractional vortex. Additionally, its amplitude A_{20} is chosen to be much lower than this of the beam carrying the dark beam ($|A_{20}| \ll |A_{10}|$). Since in the experiment both beams are delivered with the same polarization from the same laser source (at a shifted CGH), negligible influence of the second ("probe") beam on the medium nonlinearity is ensured by a quick shift of the CGH and short ($<2s$) interaction with the crystal prior the respective experimental frame is recorded.

Figure 3 presents experimental (left) and numerically simulated (right) profiles ($|A_1|^2$) of the pump beam at the exit of the SBN crystal. In the simulation, some 16% of the total computational area are shown. The experiment and the numerical simulations are in good qualitative agreement. One can clearly see that the deflection of the fractional vortex
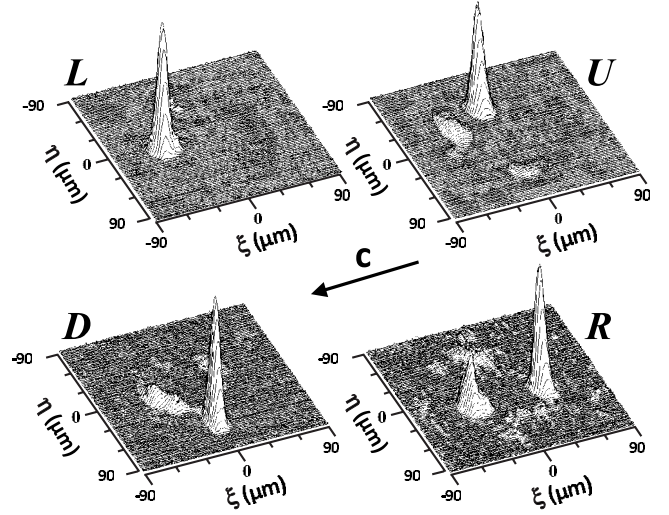

FIG. 4. Experimental results. Surface plots of the deflected signal beams at the exit of the SBN crystal for four different orientations of the CGH.

dipole causes the formation of a bright peak that is self-focused in the course of its nonlinear evolution. As a result, curved optically induced waveguide is written in the crystal. In Fig. 4, we show surface plots of the experimentally recorded power-density distributions of the guided signal beam for different orientations of the CGH. Here the transverse Cartesian coordinates ξ and η are used in order to avoid confusion with the adopted notations in which the one-dimensional part of the dislocation is along the x axis and the vortex dipole is moving parallel to the y axis. As seen in Fig. 4, four virtual output channels can be clearly distinguished. They are marked with L (left), R (right), U (up), and D (down). In the upper left frame L, the carrier drift coincides with the deflection direction and therefore contributes positively to the guiding efficiency. In the remaining three frames, however, there is a cross-talk signal guided along the crystalline c axis.

Figure 5(a) shows the orientations of the CGHs for addressing the respective output channels and Fig. 5(b) presents a composite image of all four deflected beams. According to our notation, in Table I we summarize the estimated guiding efficiencies for each channel. The guiding efficiency $\mathcal{E}_G$ is defined as the probe beam intensity $|A_2|^2$ directed at the exit of the nonlinear medium ($z = z_{NL} = 2.5L_{\text{Diff}}$) to the respective channel, integrated in time (within the integration win-
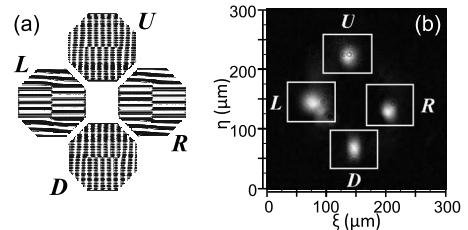

FIG. 5. (a) Sketch of the orientation of the CGH for addressing the four virtual output channels. (b) Composite image of all four deflected beams. The virtual output channels (100×80 pix) are marked with L (left), R (right), U (up), and D (down).

TABLE I. Efficiency of guiding to the four virtual output channels, as marked in Fig. 5(b).

Addressed channel	Guiding efficiency in channel			
	U	L	D	R
U	**47%**	7%	5%	2%
L	9%	**49%**	3%	6%
D	3%	12%	**38%**	4%
R	7%	18%	4%	**30%**

dow ΔT of the CCD camera) and in space (within the virtual output channel cross section), divided by the same quantity at the entrance of the NLM ($z=0$; when the lens L_3 and the CCD are shifted to image the crystal's input facet), integrated over the whole CCD-camera array

$$\mathcal{E}_G = \frac{\iint_{S_{R,U,D,L}} \int_{\Delta T} |A_2(z=z_{NL})|^2 d\tau d\xi d\eta}{\iint_{S_{CCD}} \int_{\Delta T} |A_2(z=0)|^2 d\tau dS}. \quad (7)$$

Here, $d\xi \in [-50 \text{ pix}, 50 \text{ pix}]$, $d\eta \in [-40 \text{ pix}, 40 \text{ pix}]$, and $S_{CCD}=768 \times 512 \text{ pix}^2$. The results in Table I show reasonable efficiency in the main channel, with contrast between the signal in the addressed and the remaining channels higher than 6.7, 5.4, 3.2, and 1.7 for the U, L, D, and R channels, respectively. The highest guiding efficiency (49%) was estimated when the probe beam deflection is along the crystalline c axis, whereas the deflection in the opposite direction has the lowest efficiency of 30%. While these data correspond to the particular parameters of the experiment, in general, the transverse velocity of the beam $V_\perp$ depends on both the dislocation length $2b$ and the magnitude of the phase jump $\Delta\Phi$. Therefore, by optimizing these geometrical parameters, one can further enhance the beam deflection over a particular crystal length.

Typical numerical results obtained for the intensity $|A_2|^2$ of the probe wave by solving Eqs. (2) and (3) are shown in Fig. 6. The distance CGH to NLM, needed in the experiment to filter the first diffraction order after the CGH, is modeled by linear beam propagation of $z=7.5L_{Diff}$, while the nonlinear propagation length inside the SBN crystal is over $2.5L_{Diff}$.

The numerical results agree qualitatively well with our experiments. Quantitatively, the photorefractive anisotropy and the beam modulational instability are gradually stronger pronounced in the numerical results as compared to the experimental data. Similar to the experiment, the clearest deflection, with the highest contrast between the channels, was obtained in the case when the beam steering direction coincides with the direction of the carrier drift along with the crystalline c axis (see plot L in Fig. 6). Nevertheless, second peak self-focusing at a smaller growth rate is clearly visible. When the direction of the beam steering is reversed (see plot R in Fig. 6), the signal guided to the opposite right channel still dominates. However, it appears split and with a weaker
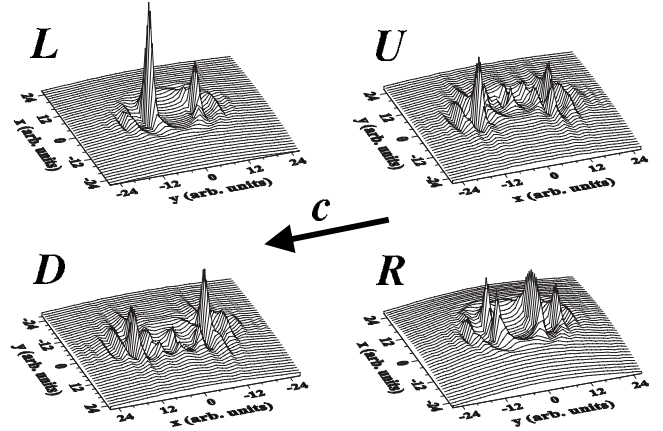

FIG. 6. Calculated intensity distributions ($|A_2|^2$) of the deflected probe beams at the exit of the crystal for $\Delta\Phi=\pi$ and $2b=35$ μm. For better visibility, plot L is scaled by a factor of 2.

growth rate in the simulations. This is only in a qualitative agreement with the experimental observation shown in Fig. 4 (R). When steering the waveguide perpendicular to the crystalline c axis, the beam in the experimental frames [Fig. 4 (U,D)] is somewhat disturbed along the c axis and opposite to the deflection direction. This is much stronger expressed in the numerical results in which the dominating peaks are actually located along the c axis. Increasing the numerical propagation distance, the bright peaks continue to self-focus and the guided probe beam becomes stronger deflected and focused (in channel L) or splitted (in the other channels). In the experiment, lengthening the interaction time of the fractional vortex dipole with the crystal results in stronger self-focusing of the bright peak and in a stronger confinement of the guided probe beam at the exit of the crystal without noticeable beam breakup. Beyond the crystal, of course, the beams diffract stronger. In agreement with earlier results obtained in self-defocusing Kerr NLM [25,27], the numerical data confirmed that the transverse velocity $V_\perp$ of the fractional vortex dipole (as well as $V_\perp$ of the bright peaks) depend inversely proportional to the dislocation length $2b$, whereas the modulational instability increases with $2b$.

IV. CONCLUSION

In conclusion, we reported on the first experimental demonstration of signal beam deflection by steering fractional vortex dipole with a mixed phase dislocation of a finite length in a self-focusing nonlinear medium. We observed high contrast between the signals guided to four desired output channels obtained with rotation of the encoded phase dislocation. Such rotation is easily achievable through the use of a programmable spatial light modulator and therefore the proposed steering scheme appears promising for realization of all-optical beam deflection. Furthermore, the observed

[1] G. I. Stegeman and M. Segev, Science **286**, 1518 (1999).

[2] Yu. S. Kivshar and B. Luther-Davies, Phys. Rep. **298**, 81 (1998).

[3] R. De La Fuente, A. Barthelemy, and C. Froehly, Opt. Lett. **16**, 793 (1991).

[4] A. W. Snyder and A. P. Sheppard, Opt. Lett. **18**, 482 (1993).

[5] P. Mamyshev, A. Villeneuve, G. Stegeman, and J. Aitchison, Electron. Lett. **30**, 726 (1994).

[6] L. L. Friedrich, G. I. Stegeman, P. Millar, C. J. Hamilton, and J. S. Aitchison, Opt. Lett. **23**, 1438 (1998).

[7] Y. Li, D. Y. Chen, L. Yang, and R. R. Alfano, Opt. Lett. **16**, 438 (1991).

[8] J. F. Nye and M. V. Berry, Proc. R. Soc. London, Ser. A **336**, 165 (1974).

[9] L. Allen, M. J. Padgett, and M. Babiker, Prog. Opt. **39**, 291 (1999).

[10] G. A. Swartzlander, Jr. and C. T. Law, Phys. Rev. Lett. **69**, 2503 (1992).

[11] A. S. Desyatnikov, Yu. S. Kivshar, and L. Torner, in *Optics*, edited by E. Wolf (North-Holland, Amsterdam, 2005), Vol. 47.

[12] Z. Chen, M.-F. Shih, M. Segev, D. W. Wilson, R. E. Muller, and P. D. Maker, Opt. Lett. **22**, 1751 (1997).

[13] A. H. Carlsson, J. N. Malmberg, D. Anderson, M. Lisak, E. A. Ostrovskaya, T. J. Alexander, and Yu. S. Kivshar, Opt. Lett. **25**, 660 (2000).

[14] C. T. Law, X. Zhang, and G. A. Swartzlander, Opt. Lett. **25**, 55 (2000).

[15] Yu. S. Kivshar, J. Christou, V. Tikhonenko, B. Luther-Davies, and L. M. Pismen, Opt. Commun. **152**, 198 (1998).

[16] D. Rozas, C. T. Law, and G. A. Swartzlander, Jr., J. Opt. Soc. Am. B **14**, 3054 (1997).

[17] B. Luther-Davies, R. Powles, and V. Tikhonenko, Opt. Lett. **19**, 1816 (1994).

[18] D. Neshev, A. Dreischuh, M. Assa, and S. Dinev, Opt. Commun. **151**, 413 (1998).

[19] D. Neshev, A. Dreischuh, S. Dinev, and L. Windholz, J. Opt. Soc. Am. B **14**, 2869 (1997).

[20] A. Dreischuh, V. Kamenov, and S. Dinev, Appl. Phys. B: Lasers Opt. **63**, 145 (1996).

[21] V. Kamenov, A. Dreischuh, and S. Dinev, Phys. Scr. **55**, 68 (1997).

[22] A. Dreischuh, D. Neshev, G. G. Paulus, F. Grasbon, and H. Walther, Phys. Rev. E **66**, 066611 (2002).

[23] A. V. Mamaev, M. Saffman, and A. A. Zozulya, Phys. Rev. Lett. **78**, 2108 (1997).

[24] A. Dreischuh, G. G. Paulus, and F. Zacher, Appl. Phys. B: Lasers Opt. **69**, 107 (1999).

[25] A. Dreischuh, G. G. Paulus, F. Zacher, and I. Velchev, Appl. Phys. B: Lasers Opt. **69**, 113 (1999).

[26] D. Neshev, A. Dreischuh, G. G. Paulus, and H. Walther, Appl. Phys. B: Lasers Opt. **72**, 849 (2001).

[27] K. Bezuhanov and A. Dreischuh, Proc. SPIE **5830**, 211 (2005).

[28] V. Tikhonenko, J. Christou, and B. Luther-Davies, J. Opt. Soc. Am. B **12**, 2046 (1995).

[29] W. J. Firth and D. V. Skryabin, Phys. Rev. Lett. **79**, 2450 (1997).

[30] L. Torner and D. V. Petrov, Electron. Lett. **33**, 608 (1997).

[31] L. T. Vuong, T. D. Grow, A. Ishaaya, A. L. Gaeta, G. W. tHooft, E. R. Eliel, and G. Fibich, Phys. Rev. Lett. **96**, 133901 (2006).

[32] M. Morin, G. Duree, G. Salamo, and M. Segev, Opt. Lett. **20**, 2066 (1995).

[33] A. Stepken, M. R. Belic, F. Kaiser, W. Krolikowski, and B. Luther-Davies, Phys. Rev. Lett. **82**, 540 (1999).

[34] A. Zakery and A. Keshavarz, J. Phys. D **37**, 3409 (2004).

[35] M.-F. Shih, M. Segev, and G. Salamo, Phys. Rev. Lett. **78**, 2551 (1997).

[36] W. Królikowski, M. Saffman, B. Luther-Davies, and C. Denz, Phys. Rev. Lett. **80**, 3240 (1998).